Author/s:
Luo, Z;Pederick, VG;Paton, JC;McDevitt, CA;Kobe, B

Title:
Structural characterisation of the HT3 motif of the polyhistidine triad protein D from Streptococcus pneumoniae

Date:
2018-07-01

Citation:
Luo, Z., Pederick, V. G., Paton, J. C., McDevitt, C. A. & Kobe, B. (2018). Structural characterisation of the HT3 motif of the polyhistidine triad protein D from Streptococcus pneumoniae. FEBS Letters, 592 (13), pp.2341-2350. https://doi.org/10.1002/1873-3468.13122.

Persistent Link:
https://hdl.handle.net/11343/284167

Received Date : 24-Apr-2018
Revised Date : 11-May-2018
Accepted Date : 21-May-2018
Article type : Research Letter

Corresponding author mail id: b.kobe@uq.edu.au

Structural characterisation of the HT3 motif of the polyhistidine triad protein D from *Streptococcus pneumoniae*

Zhenyao Luo[1,2,3], Victoria G. Pederick[4], James C. Paton[4], Christopher A. McDevitt[4], Bostjan Kobe[1,2,3*]

1. School of Chemistry and Molecular Biosciences, University of Queensland, Brisbane, Queensland, Australia.
2. Australian Infectious Diseases Research Centre, University of Queensland, Brisbane, Queensland, Australia.
3. Institute for Molecular Bioscience, University of Queensland, Brisbane, Queensland, Australia.
4. Research Centre for Infectious Diseases, School of Biological Sciences, University of Adelaide, Adelaide, South Australia, Australia.

ABSTRACT

The bacterium *Streptococcus pneumoniae* (the pneumococcus) is a major human pathogen that requires Zn^{2+} for its survival and virulence in the host environment. Polyhistidine triad protein D (PhtD) has a known role in pneumococcal Zn^{2+}

homeostasis. However, the mechanistic basis of PhtD function remains unclear, partly due to a lack of structural information. Here, we determined the crystal structure of the fragment PhtD$^{269-339}$, containing the third Zn^{2+}-binding histidine triad (HT) motif of the protein. Analysis of the structure suggests that Zn^{2+}-binding occurs at the surface of the protein and that all five HT motifs in the protein bind Zn^{2+} and share similar structures. These new structural insights aid in our understanding of how the Pht proteins facilitate pneumococcal Zn^{2+} acquisition.

ABBREVIATIONS

HT, histidine triad

Pht, polyhistidine triad

SBP, solute-binding protein

KEYWORDS (up to six)

Streptococcus pneumoniae, zinc acquisition, polyhistidine triad, PhtD, *in situ* proteolysis, x-ray crystallography

INTRODUCTION

The bacterium *Streptococcus pneumoniae* (the pneumococcus) is a major human pathogen associated with significant global morbidity and mortality [1]. Although the pneumococcus is a common commensal of the human nasopharynx [2], it can invade other tissues including the lungs, brain, and ears, where it is associated with a broad spectrum of diseases, ranging from local infections, such as otitis media, to invasive diseases including pneumonia and meningitis [3,4]. Zinc (Zn^{2+}) is an essential nutrient for *S. pneumoniae* and the ability to acquire this trace metal at the host-pathogen interface is critical for survival of the bacterium. Acquisition of Zn^{2+} by *S. pneumoniae* is primarily facilitated by the ATP-binding cassette transporter, AdcCB,

and two Zn^{2+}-specific solute-binding proteins (SBPs), AdcA and AdcAII [5,6]. Abrogation of Adc permease function severely impacts Zn^{2+} uptake and attenuates pneumococcal virulence in murine models of infection [5,6].

During Zn^{2+}-starvation, the pneumococcus up-regulates a large number of genes, including those encoding surface proteins of the histidine triad (HT) family [7]. This family of proteins is found throughout the *Streptococcus* genus, although there are exceptions, with the defining feature of repeated HT (HxxHxH) motifs [8]. *S. pneumoniae* encodes four Pht proteins, PhtA, PhtB, PhtD, and PhtE [9], which range from 90 to 116 kDa in size. Transcription of the Pht genes is tightly regulated by the Zn^{2+}-responsive metalloregulator AdcR and they are co-expressed with the Zn^{2+}-specific SBP *adcAII* [10-12]. The co-regulation of *adcAII* with *phtD* led to the *pht* genes being implicated in divalent cation scavenging by *S. pneumoniae* [13].

Subsequent studies revealed that the Pht proteins primarily localise to the pneumococcal cell wall, but could also be observed secreted in the extracellular medium [9,14], and contributed specifically to Zn^{2+} homeostasis and pneumococcus virulence [11,15]. Intriguingly, the role of the Pht proteins in Zn^{2+} homeostasis was shown to be facilitated by AdcAII, with negligible dependence upon the other SBP, AdcA.

Interaction between AdcAII and PhtD has been probed and although interaction has been shown *in vitro* [16], direct evidence of *in vivo* Zn^{2+} transfer from the Pht proteins to AdcAII remains elusive. Further challenging elucidation of the molecular basis of Pht protein function is the overlapping functionality of the proteins, with only a single Pht isoform necessary for pneumococcal growth [11]. Another major issue that has precluded detailed insights into the Pht proteins has been the paucity of structural data. This has largely been attributed to the intrinsic flexibility of these protein molecules, as suggested by secondary and tertiary structure predictions. Moreover, full-length PhtD is prone to degradation and techniques such as small angle X-ray scattering have not been successful in providing structural insights about the protein in solution. However, significant advances have been achieved, notably by Riboldi-Tunnicliffe *et al.* [17], who reported the crystal structure at 1.2 Å resolution of a 55-residue fragment from pneumococcal PhtA, which contained the HT2 motif. In this structure, Zn^{2+} is bound by three histidine residues from the HT motif and one glutamate residue from a nearby loop, giving a tetrahedral Zn^{2+} coordination geometry. More recently, Bersch *et al*. [12] determined the solution

structure, by nuclear magnetic resonance (NMR) spectroscopy, of a 137-residue-long N-terminal region of pneumococcal PhtD that contained the HT1 motif. This revealed a Zn^{2+} ion bound to the HT motif, using the same Zn^{2+}-binding mode as seen in the PhtA crystal structure.

The highly exposed cellular location of the Pht proteins has also attracted significant interest in this family as potential vaccine targets [18,19]. Many of the Pht protein studies have focused on examining their potential to serve as vaccine antigens for protection against pneumococcal infections [20], with some reported cases of clinical benefit [21,22]. However, the mechanistic basis of Pht protein function has remained unanswered.

Here, we structurally examined PhtD, the most highly conserved Pht protein across pneumococcal serotypes [15], using an *in situ* proteolysis approach and Zn^{2+}-SAD phasing. We report the crystal structure of a 71-residue PhtD fragment encompassing the HT3 motif (comprising residues 269-339, $PhtD^{269-339}$). Based on this structure, we then performed homology modelling of the regions containing the HT2, HT4, and HT5 motifs of PhtD. Our results suggest that all 5 HT motifs in PhtD possess similar core structural elements and have the capacity to bind Zn^{2+}, which has implications for the function of the full-length protein.

METHODS AND MATERIALS

Expression and purification

Recombinant PhtD was generated by PCR amplification of the SPD_0889 gene from Serotype 2 *S. pneumoniae* D39, using ligation-independent cloning and PhtD_LIC1F (5' TGGGTGGTGGATTTCCTGTCAGTAAGAGAGAGGGGAT) and PhtD_LIC1R (5' TTGGAAGTATAAATTTCCCTGTATAGGAGTCGGTTGACT) oligonucleotides, to insert the gene into an N-terminal dodecahistidine tag-containing vector, pCAMnLIC01, to generate pCAMnLIC01-PhtD. Recombinant expression of PhtD was performed in 2 x terrific broth + 1% glucose, at 37 ºC in High-Yield Flasks (Thomson Scientific). Expression was induced at an OD_{600} of 3.0 using isopropyl β-D-1-thiogalactopyranoside, and cells harvested after 4 h. Recombinant PhtD was initially isolated by virtue of its dodecahistidine tag using immobilised metal ion affinity chromatography on a HisTrapHP Column using an AKTA Fast Protein Liquid Chromatography (FPLC) System (GE Healthcare). The tag was then removed by

incubation with a human rhinovirus C3 protease at a ratio of 10:1 (protein:protease) and purification of the cleaved protein on a HisTrapHP column. To further purify the protein, PhtD was subjected to anion-exchange chromatography using a HiTrapQ HP column (GE Healthcare), followed by gel-permeation chromatography on a HiLoad 16/60 Superdex 200 PG column (GE Healthcare) in 20 mM Tris (pH 7.6) and 200 mM NaCl on an AKTA FPLC.

Crystallisation

Purified recombinant PhtD protein was concentrated to 20 mg/ml using a centrifugal filter unit (Amicon MWCO 10 kDa, Millipore). Crystals were obtained using the hanging drop vapour diffusion method at 20 °C in 1.1 M sodium malonate, 0.5 % (v/v) JED-2003, and 0.1 M HEPES-NaOH pH 7.0, in the presence of α-chymotrypsin (1 μg protease per 100 μg PhtD) (Sigma C3142) in the crystallisation drops, taking advantage of *in situ* proteolysis of PhtD. α-Chymotrypsin solution was prepared as described in Dong *et al*. [23].

Data collection, processing and structure determination

Crystals were mounted onto CryoLoops (Hampton Research) and were briefly soaked in Paratone-N (Hampton Research) before being flash-cooled in liquid nitrogen. Prior to data collection, a fluorescence excitation scan was performed to confirm the presence of Zn^{2+} in the crystals. The X-ray diffraction data was collected from a single crystal using X-ray radiation energy at 9858 eV at the Australian Synchrotron MX1 beamline [24], with a rotation range of 360°, using 0.5° oscillations and 1 second X-ray exposures per diffraction image. The collected data was indexed and integrated using *XDS* [25] and scaled and merged using *Aimless* [26]. The Friedel pairs were kept separated during data processing. Initial experimental phases were calculated using *AutoSol* [27] and the initial model was constructed using *Phenix.AutoBuild* [28]. The structure was refined iteratively using *Phenix.Refine* [29] and manually corrected in *COOT* [30].

Homology modelling

Homology models of the PhtD fragments containing the HT2, HT4, and HT5 motifs were constructed using the crystal structure obtained in this study as the template using *Modeller 9.19* [31]. The secondary structure of PhtD was predicted using

PHYRE2 [32] and JPred4 [33]. Sequence alignment was performed using EMBOSS Needle [34], with manual adjustments based on the secondary structure prediction. The region of PhtD for each modelled HT-containing fragment was as follows: HT2 fragment, residues 159-231; HT4 fragment, residues 515-586; HT5 fragment, residues 598-670.

RESULTS

Determination of the crystal structure of PhtD$^{269\text{-}339}$

We initially sought to crystallise full-length pneumococcal PhtD; however, the protein was refractory to crystallisation. We therefore used *in situ* proteolysis, which has previously been shown as a rescue technique to crystallise proteins [23,35,36]. The approach takes advantage of the proteolytic products of larger proteins with higher crystallization propensities that are generated. Here, we employed the protease α-chymotrypsin, which was supplemented in the crystallisation drops containing full-length PhtD. Three weeks after setup, single crystals started to appear in the crystallisation drops.

Data collection at the Australian Synchrotron confirmed the presence of Zn^{2+}, based on a fluorescence excitation scan; a fluorescence peak corresponding to the emission energy of Zn^{2+} ion at approximately 8638 eV was observed. We subsequently used the Zn^{2+} present in the crystal as an anomalous scatterer and collected diffraction data at the Zn^{2+} *Kα* edge around 9858 eV, to optimise the anomalous signal from Zn^{2+}. The merged data had a mid-slope of anomalous normal probability of 1.7, indicating a strong anomalous signal present in the diffraction data. The PhtD fragment crystals had the symmetry of space group C2 with a monoclinic unit cell (a = 59.03 Å, b = 47.98 Å, c = 23.59 Å, α = 90.00 °, β = 107.13 °, γ = 90.00 °). A single copy of the PhtD fragment was present in each asymmetric unit. The electron density map was calculated using phases derived from the Zn^{2+} anomalous signal and the structure was determined to a resolution of 1.92 Å. Details of diffraction and structure statistics are summarised in Table 1.

We attempted to determine the precise region of the crystallised PhtD fragment using mass spectroscopy. However, the results were inconclusive due to contamination of the crystals with other PhtD peptides. SDS-PAGE using dissolved crystals (data not shown) revealed a protein band below 10 kDa. Using PeptideCutter

[37], a cleavage prediction tool, the region most likely cleaved by α-chymotrypsin corresponds to residues 266-341, with a calculated molecular weight of 8636 Da, which is consistent with the estimated fragment size by SDS-PAGE. However, based on the electron density map, only residues 269-339 can be modelled unambiguously, and therefore the fragment is denoted as PhtD$^{269-339}$.

Overall structure of PhtD$^{269-339}$

The crystal structure of the 71-residue PhtD$^{269-339}$ consists of a globular bundle of two short α-helices and three anti-parallel β-strands **(Figure 1A, B**). Helix α1 (residues 270-282) and β-strand β1 (residues 303-305) are connected by a long loop α1β1 (residues 283-302), with the rest of the secondary structure elements connected by short loops. Analysis of the surface electrostatic potential shows an uneven charge distribution on the PhtD$^{269-339}$ surface (**Figure 1C**). The fragment contains the HT3 region of pneumococcal PhtD, comprising His314 residing on β-strand β2 (residues 309-314), and His317 and His319 on β-strand β3 (residues 317-322). β2 and β3 form a β-hairpin motif, which brings His314, His317, and His319 to close proximity. A Zn^{2+}-binding site is formed by these three histidine residues and an aspartic acid residue, Asp293, from loop α1β1. Notably, the Zn^{2+}-binding site resides on the surface of the protein fragment, with immediate access for Zn^{2+} from the surrounding solvent to the binding site. In the binding site, a Zn^{2+} ion is bound by the atoms Nδ1 from His314, Nε2 from His317, Nε2 from His319, and Oδ2 from Asp293 in a tetrahedral coordination geometry (**Figure 2**), with coordination bond angles of 105.5 °, 107.4 °, 108.4 °, and 110.0 °, respectively. The observed bond lengths are 1.98 Å, 2.09 Å, 2.02 Å, and 1.97 Å, respectively, and are typical for protein coordination of a Zn^{2+} ion [38]. The Zn^{2+}-binding region, along with the rest of the exposed loop α1β1, exhibits a negatively-charged surface, while the helical region presents a positively-charged surface. Although loop α1β1 appears to be ordered in the structure, the mobility of this region may increase in the absence of the ion and the stabilising interaction conferred by Asp293.

Structural comparisons of PhtD$^{269-339}$ with PhtD$^{40-158}$ and PhtA$^{166-220}$

We compared the PhtD$^{269-339}$ structure determined in this work with the structures of the *S. pneumoniae* Pht protein fragments PhtA$^{166-220}$, obtained by crystallography [17] that encompasses the HT2 motif of PhtA, and PhtD$^{40-158}$, an NMR solution structure

of the N-terminal region [12] that contains the HT1 motif of PhtD. Sequence comparisons show that PhtD$^{269-339}$ and PhtA$^{166-220}$ share approximately 30% sequence identity, with the HT motifs completely conserved. Superposition of the two structures generates a root-mean-square deviation of 0.69 Å over 55 C_α atoms. Overall, despite the low sequence identity, the two structures show a conserved structural fold, including all the three β-strands, α2, and the Zn^{2+}-binding site defined by the HT motif and an aspartic acid residue from loop α1β1 (**Figure 3A**). The Zn^{2+} coordination in the binding site in both structures is also highly similar, with comparable coordination bond lengths. By contrast, PhtD$^{40-158}$ and PhtD$^{269-339}$ share only 17% sequence identity, with the two structures showing a number of distinct features. In PhtD$^{40-158}$, an α-helix is present in the loop that corresponds to the α1β1 region in PhtD$^{269-339}$; the first β-strand in PhtD$^{40-158}$ is twice the length of the equivalent region in PhtD$^{269-339}$; and the α1 and α2 helices found in PhtD$^{269-339}$ are absent in PhtD$^{40-158}$. Notably, the Zn^{2+}-coordinating carboxylate residue in PhtD$^{40-158}$, Glu63, is situated on the α-helix present in the loop, which corresponds to α1β1 region in PhtD$^{269-339}$. However, despite these differences, the structures of the Zn^{2+}-binding sites are highly conserved, featuring the histidine triad residing on a β-hairpin and a negatively charged residue that defines a tetrahedral Zn^{2+}-coordination environment (**Figure 3B**).

Homology models of the PhtD HT motifs suggest similar Zn^{2+}-binding mechanisms

Secondary-structure prediction of PhtD shows that regions encompassing HT2, HT3, HT4, and HT5 motifs (when including 40 residues before and 20 residues after the HT motif in the analysis) all contain similar secondary-structure features, including the two β-strands harbouring the HT motif, and at least one of the two helices, despite low sequence identities (34.2%, 28.8%, and 21% of the HT2, HT4, and HT5 containing fragments, compared with PhtD$^{247-317}$, respectively). Homology modelling of HT2, HT4, and HT5 using PhtD$^{269-339}$ as the template revealed that all HT models adopt a similar structural fold, with the capacity of binding Zn^{2+} in the solvent-accessible Zn^{2+}-binding site defined by the HT motifs (**Figure 4**). Examination of the surface electrostatic potentials of all the 5 HT motif-containing regions of PhtD suggests that all motifs include charged surfaces (**Figure 5**), which are likely to be exposed on the surface of PhtD protein.

DISCUSSION

Acquisition of Zn^{2+} from the host environment is essential for the ability of *S. pneumoniae* to colonize and mediate disease. PhtD has been shown to aid in pneumococcal pathogenesis via the acquisition of Zn^{2+} during growth in Zn^{2+}-limiting conditions, while also aiding in resisting host clearance via binding Factor H [10,15,39]. Although the *in vivo* significance of the Pht proteins in resisting complement-mediated clearance remains unclear, their contribution to Zn^{2+} acquisition, facilitated primarily in association with AdcAII, is well established [5,16]. Despite this, the molecular basis for how PhtD contributes to Zn^{2+} acquisition remains unclear, due to a lack of structural information on the histidine-triad family proteins. Prior to this work, the N-terminal region of PhtD, which contains the HT1 motif, was the only portion of this protein with structural information. Here, we determined the high-resolution structure of $PhtD^{269\text{-}339}$, containing the HT3 motif of pneumococcal PhtD, providing new insights into Zn^{2+} recruitment by the histidine triad motifs.

Although full-length PhtD remains refractory to crystallisation, by combining our high-resolution structural analysis of $PhtD^{269\text{-}339}$ with homology modelling of the other three HT-containing regions, we can speculate reasonably on potential mechanistic aspects of PhtD function. Here, our comparison of the HT motifs suggests that they likely share a conserved tertiary structure similar to HT3, most notably in their respective Zn^{2+}-binding sites. Loisel *et al.* [16] reported the affinity of the PhtD HT1 for Zn^{2+} as 131 ± 10 nM. Given the structural similarities of all HT motifs in PhtD, we speculate that binding affinities of other HT motifs would be comparable to that of HT1. However, in a complex protein, such as PhtD, it is not unreasonable to expect cooperativity between the HT motifs and allosteric interactions between sites that may influence Zn^{2+} binding. Recent work by Eijkelkamp *et al*. [15] revealed a hierarchy for the five HT motifs of PhtD with respect to their importance for *in vitro* Zn^{2+} acquisition. That work showed that HT1 of PhtD, which is closest to the pneumococcal cell membrane, was the most important, whereas HT5 had the smallest contribution. Analysis of pneumococcal mutants lacking the HT2, HT3 or HT4 motifs of PhtD revealed an impact on Zn^{2+}

import, albeit to a lesser extent than a mutant lacking HT1. Whether these findings indicate cooperativity of binding or allosteric changes within PhtD remains to be confirmed.

The isolation of the HT3 fragment crystals by *in situ* proteolysis indicates that the HT3 fragment is exposed on the surface of PhtD, rendering it accessible to α-chymotrypsin. Furthermore, the uneven distribution of surface electrostatic potential on the HT3 fragment surface is also consistent with a solvent-exposed location. Examination of the $PhtD^{40-158}$ solution structure and the homology models of HT2, HT4, and HT5 regions reveals that, similar to $PhtD^{269-339}$, all these fragments possess charged surfaces and would suggest protein surface localisation. This structural composition would be consistent with the contribution of these motifs to Zn^{2+} acquisition at the pathogen-host interface [11,15]. Notably, the histidine triad residues in HT3 are on a β-hairpin, and as such it would be expected that the conformation of this region would be largely stable in the absence of Zn^{2+}. This arrangement suggests that the Zn^{2+}-binding site in the HT motif is essentially pre-formed. As a consequence, Zn^{2+} binding is likely to be controlled by coordination of Asp293 from the α1β1 loop, with the resultant movement of the α1β1 loop towards the β-hairpin, thereby excluding the Zn^{2+} ion from the solvent. PhtD binding to Zn^{2+} has been shown by fluorescence quenching experiments to decrease the exposure of tryptophan residues to the solvent [40]. Taken together, these observations suggest that the conformational changes induced by Zn^{2+} binding at the HT sites also affect the overall structure of PhtD. One possible functional implication of this process would be to enable the formation of a cascade of HT sites across the cell wall and thereby provide a pathway for Zn^{2+} translocation to the pneumococcal cell membrane. Analysis of the C-terminal region of PhtD, distal to the pneumococcal cell wall and closer to the host cells, reveals that this region comprises multiple histidine residues and is highly packed with negatively charged residues. In essence, this region resembles the highly flexible histidine-rich loop in the Adc permease associated Zn^{2+}-binding protein AdcA [5]. In AdcA, this region is proposed to act as a mobile Zn^{2+} scavenger that aids in the delivery of the captured metal ion to the binding site of AdcA [5]. The C-terminal domain of PhtD may hold a similar function and transfer the captured Zn^{2+} to the HT motifs, enabling the transfer from the host environment to AdcAII at the pneumococcal cell surface.

In summary, we present the crystal structure of PhtD$^{269-339}$, harbouring the HT3 motif of pneumococcal PhtD, providing new structural insights into this challenging family of proteins. Structural examination of HT3 indicates that binding of Zn^{2+} most likely occurs at the surface of the protein and that this process is likely coupled to broader structural changes. Together, the combination of Zn^{2+}-binding strategies enhances the acquisition of this essential ion by *S. pneumoniae*.

DATA DEPOSITION

Coordinates of the PhtD$^{269-339}$ fragment crystal structure have been deposited in the Protein Data Bank with accession code 6CSL.

ACKNOWLEDGMENTS

We acknowledge the use of the UQ-ROCX Facility and the Australian Synchrotron MX beamlines. This work was supported by the National Health and Medical Research Council (NHMRC) Program Grant 1071659 to B.K. and J.C.P. and Project Grants 1080784 and 1122582 to C.A.M. This work was also supported by the ARC Discovery Project DP170102102 to C.A.M. and J.C.P.. C.A.M. is an ARC Future Fellow (FT170100006) and B.K. is an NHMRC Principal Research Fellow (1110971).

Figure 1. Crystal structure of pneumococcal PhtD$^{269-339}$. (A) Sequence and crystal structure-based secondary structure of pneumococcal PhtD$^{269-339}$. The α-helices are shown as red cylinders and β-strands are shown as yellow arrows. The Zn^{2+}-coordinating residues are coloured in blue. Numbers of the starting and ending residues are indicated in the sequence using superscript. (B) Cartoon representation of PhtD$^{269-339}$ crystal structure. The α-helices are coloured in red, β-strands in yellow, and loops in green. The bound Zn^{2+} ion is shown as a white sphere and its coordinating residues as cyan sticks. (C) Surface electrostatic potential of PhtD$^{269-339}$ crystal structure shown in the same orientation as in (B). Positive and negative potentials are shown in blue and red, respectively, coloured continuously between -5 and 5 kT/e. Surface electrostatic potential was calculated using APBS [41]; the

calculation included the Zn^{2+} ions. The N- and C- termini of the structure are indicated by 'N' and 'C', respectively.

Figure 2. The Zn^{2+}-binding site of pneumococcal $PhtD^{269-339}$. The Zn^{2+} ion is shown as a white sphere. The Zn^{2+}-coordinating residues are shown as cyan sticks, with the atoms contributing to the interactions as spheres. The coordinating bonds are illustrated with black dashed lines. The electron density shown is the $2F_o$-F_c map contoured at 1.5 σ.

Figure 3. Structural comparison of $PhtD^{269-339}$ with $PhtA^{166-220}$ and $PhtD^{40-158}$. (A) Superposition of the crystal structure of $PhtD^{269-339}$ (green) and $PhtA^{166-220}$ (cyan, PDB ID: 2CS7) [17] in cartoon representation. The bound Zn^{2+} ions are shown as spheres and the Zn^{2+}-coordinating residues are shown as sticks. (B) Superposition of the crystal structure of $PhtD^{269-339}$ (green) and the solution structure of $PhtD^{40-158}$ (magenta, PDB ID: 3ZFJ) [12] in cartoon representation. The bound Zn^{2+} ions are shown as spheres and the Zn^{2+}-coordinating residues are shown as sticks.

Figure 4. Homology models of pneumococcal HT fragments. (A) Sequence alignments of the HT2, HT3, HT4, HT5 fragments of PhtD, and the HT2 fragment of PhtA. The Zn^{2+} ion-coordinating residues are highlighted in blue and the numbers of the starting and ending residues of the respective fragment are noted using superscript. The alignment was prepared using Clustal Omega [42]. (B) HT2-containing fragment model shown in green cartoon representation. (C) HT4-containing fragment model shown in cyan cartoon representation. (D) HT5-containing fragment model shown in magenta cartoon representation. The bound Zn^{2+} ions are shown as white spheres and their coordinating-residues are shown in stick representation. Secondary structure prediction for each HT fragment is shown below

each model. α-Helices are indicated by red cylinders, β-strands are represented by yellow arrows, and the Zn^{2+}-coordinating residues are coloured in cyan.

Figure 5. Surface electrostatic potential of pneumococcal HT-containing fragments. Molecules are shown in surface representation, coloured according to electrostatic potential. Positive and negative potentials are shown in blue and red, respectively, coloured continuously between -5 and 5 kT/e. Surface electrostatic potential was calculated using APBS [41] ; the calculation included the Zn^{2+} ions. The positions of the Zn^{2+}-binding sites are indicated. For HT1, the solution structure of $PhtD^{40-158}$ was used (PDB ID: 3ZFJ) [12]. For HT3, the crystal structure of $PhtD^{269-339}$ was used. For HT2, HT4, and HT5, the homology models generated in this study were used.

REFERENCES

[1] McDevitt, C.A., Ogunniyi, A.D., Valkov, E., Lawrence, M.C., Kobe, B., McEwan, A.G. and Paton, J.C. (2011). A molecular mechanism for bacterial susceptibility to zinc. PLoS Pathog 7, e1002357.

[2] Kadioglu, A., Weiser, J.N., Paton, J.C. and Andrew, P.W. (2008). The role of *Streptococcus pneumoniae* virulence factors in host respiratory colonization and disease. Nat Rev Microbiol 6, 288-301.

[3] Paton, J.C. (1998). Novel pneumococcal surface proteins: role in virulence and vaccine potential. Trends Microbiol 6, 85-7; discussion 87-8.

[4] O'Brien, K.L. et al. (2009). Burden of disease caused by *Streptococcus pneumoniae* in children younger than 5 years: global estimates. Lancet 374, 893-902.

[5] Plumptre, C.D. et al. (2014). AdcA and AdcAII employ distinct zinc acquisition mechanisms and contribute additively to zinc homeostasis in *Streptococcus pneumoniae*. Mol Microbiol 91, 834-51.

[6] Bayle, L., Chimalapati, S., Schoehn, G., Brown, J., Vernet, T. and Durmort, C. (2011). Zinc uptake by *Streptococcus pneumoniae* depends on both AdcA and AdcAII and is essential for normal bacterial morphology and virulence. Mol Microbiol 82, 904-16.

[7] Shafeeq, S., Kloosterman, T.G. and Kuipers, O.P. (2011). Transcriptional response of *Streptococcus pneumoniae* to Zn(2+) limitation and the repressor/activator function of AdcR. Metallomics 3, 609-18.

[8] Shao, Z.Q., Zhang, Y.M., Pan, X.Z., Wang, B. and Chen, J.Q. (2013). Insight into the evolution of the histidine triad protein (HTP) family in Streptococcus. PLoS One 8, e60116.

[9] Plumptre, C.D., Ogunniyi, A.D. and Paton, J.C. (2012). Polyhistidine triad proteins of pathogenic streptococci. Trends Microbiol 20, 485-93.

[10] Ogunniyi, A.D., Grabowicz, M., Mahdi, L.K., Cook, J., Gordon, D.L., Sadlon, T.A. and Paton, J.C. (2009). Pneumococcal histidine triad proteins are regulated by the Zn2+-dependent repressor AdcR and inhibit complement deposition through the recruitment of complement factor H. FASEB J 23, 731-8.

[11] Plumptre, C.D., Hughes, C.E., Harvey, R.M., Eijkelkamp, B.A., McDevitt, C.A. and Paton, J.C. (2014). Overlapping functionality of the Pht proteins in zinc homeostasis of *Streptococcus pneumoniae*. Infect Immun 82, 4315-24.

[12] Bersch, B., Bougault, C., Roux, L., Favier, A., Vernet, T. and Durmort, C. (2013). New insights into histidine triad proteins: solution structure of a *Streptococcus pneumoniae* PhtD domain and zinc transfer to AdcAII. PLoS One 8, e81168.

[13] Rioux, S. et al. (2011). Transcriptional regulation, occurrence and putative role of the Pht family of *Streptococcus pneumoniae*. Microbiology 157, 336-48.

[14] Plumptre, C.D., Ogunniyi, A.D. and Paton, J.C. (2013). Surface association of Pht proteins of *Streptococcus pneumoniae*. Infect Immun 81, 3644-51.

[15] Eijkelkamp, B.A., Pederick, V.G., Plumptre, C.D., Harvey, R.M., Hughes, C.E., Paton, J.C. and McDevitt, C.A. (2015). The First Histidine Triad Motif of PhtD Is Critical for Zinc Homeostasis in *Streptococcus pneumoniae*. Infect Immun 84, 407-15.

[16] Loisel, E. et al. (2011). Biochemical characterization of the histidine triad protein PhtD as a cell surface zinc-binding protein of pneumococcus. Biochemistry 50, 3551-8.

[17] Riboldi-Tunnicliffe, A., Isaacs, N.W. and Mitchell, T.J. (2005). 1.2 Angstroms crystal structure of the *S. pneumoniae* PhtA histidine triad domain a novel zinc binding fold. FEBS Lett 579, 5353-60.

[18] Adamou, J.E. et al. (2001). Identification and characterization of a novel family of pneumococcal proteins that are protective against sepsis. Infect Immun 69, 949-58.

[19] Wizemann, T.M. et al. (2001). Use of a whole genome approach to identify vaccine molecules affording protection against *Streptococcus pneumoniae* infection. Infect Immun 69, 1593-8.

[20] Plumptre, C.D., Ogunniyi, A.D. and Paton, J.C. (2013). Vaccination against *Streptococcus pneumoniae* using truncated derivatives of polyhistidine triad protein D. PLoS One 8, e78916.

[21] Godfroid, F., Hermand, P., Verlant, V., Denoel, P. and Poolman, J.T. (2011). Preclinical evaluation of the Pht proteins as potential cross-protective pneumococcal vaccine antigens. Infect Immun 79, 238-45.

[22] Prymula, R., Pazdiora, P., Traskine, M., Ruggeberg, J.U. and Borys, D. (2014). Safety and immunogenicity of an investigational vaccine containing two common pneumococcal proteins in toddlers: a phase II randomized clinical trial. Vaccine 32, 3025-34.

[23] Dong, A. et al. (2007). In situ proteolysis for protein crystallization and structure determination. Nat Methods 4, 1019-21.

[24] Cowieson, N.P. et al. (2015). MX1: a bending-magnet crystallography beamline serving both chemical and macromolecular crystallography communities at the Australian Synchrotron. J Synchrotron Radiat 22, 187-90.

[25] Kabsch, W. (2010). Xds. Acta Crystallogr D Biol Crystallogr 66, 125-32.

[26] Evans, P.R. and Murshudov, G.N. (2013). How good are my data and what is the resolution? Acta Crystallogr D Biol Crystallogr 69, 1204-14.

[27] Terwilliger, T.C. et al. (2009). Decision-making in structure solution using Bayesian estimates of map quality: the PHENIX AutoSol wizard. Acta Crystallogr D Biol Crystallogr 65, 582-601.

[28] Terwilliger, T.C., Grosse-Kunstleve, R.W., Afonine, P.V., Moriarty, N.W., Zwart, P.H., Hung, L.W., Read, R.J. and Adams, P.D. (2008). Iterative model building, structure refinement and density modification with the PHENIX AutoBuild wizard. Acta Crystallogr D Biol Crystallogr 64, 61-9.

[29] Afonine, P.V. et al. (2012). Towards automated crystallographic structure refinement with phenix.refine. Acta Crystallogr D Biol Crystallogr 68, 352-67.
[30] Emsley, P., Lohkamp, B., Scott, W.G. and Cowtan, K. (2010). Features and development of Coot. Acta Crystallogr D Biol Crystallogr 66, 486-501.
[31] Sali, A. and Blundell, T.L. (1993). Comparative protein modelling by satisfaction of spatial restraints. J Mol Biol 234, 779-815.
[32] Kelley, L.A. and Sternberg, M.J. (2009). Protein structure prediction on the Web: a case study using the Phyre server. Nat Protoc 4, 363-71.
[33] Drozdetskiy, A., Cole, C., Procter, J. and Barton, G.J. (2015). JPred4: a protein secondary structure prediction server. Nucleic Acids Res 43, W389-94.
[34] Rice, P., Longden, I. and Bleasby, A. (2000). EMBOSS: the European Molecular Biology Open Software Suite. Trends Genet 16, 276-7.
[35] Wernimont, A. and Edwards, A. (2009). In situ proteolysis to generate crystals for structure determination: an update. PLoS One 4, e5094.
[36] Tong, Y., Dong, A., Xu, X. and Wernimont, A. (2014). Salvage or recovery of failed targets by in situ proteolysis. Methods Mol Biol 1140, 179-88.
[37] Wilkins, M.R., Gasteiger, E., Bairoch, A., Sanchez, J.C., Williams, K.L., Appel, R.D. and Hochstrasser, D.F. (1999). Protein identification and analysis tools in the ExPASy server. Methods Mol Biol 112, 531-52.
[38] Laitaoja, M., Valjakka, J. and Janis, J. (2013). Zinc coordination spheres in protein structures. Inorg Chem 52, 10983-91.
[39] Melin, M., Jarva, H., Siira, L., Meri, S., Kayhty, H. and Vakevainen, M. (2009). *Streptococcus pneumoniae* capsular serotype 19F is more resistant to C3 deposition and less sensitive to opsonophagocytosis than serotype 6B. Infect Immun 77, 676-84.
[40] Ausar, S.F., Jayasundara, K., Akawi, L., Roque, C., Sheung, A., Hu, J., Kirkitadze, M. and Rahman, N. (2017). Biophysical Characterization and Thermal Stability of Pneumococcal Histidine Triad Protein D in the Presence of Zinc and Manganese. J Pharm Sci 106, 2979-2987.
[41] Baker, N.A., Sept, D., Joseph, S., Holst, M.J. and McCammon, J.A. (2001). Electrostatics of nanosystems: application to microtubules and the ribosome. Proc Natl Acad Sci U S A 98, 10037-41.

[42] Sievers, F. et al. (2011). Fast, scalable generation of high-quality protein multiple sequence alignments using Clustal Omega. Mol Syst Biol 7, 539.

Table 1. Data collection, processing, and refinement statistics.

Data collection	
Diffraction source	Australian Synchrotron MX1 Beamline
Wavelength (Å)	1.25
Resolution range (Å)	18.27-1.92 (1.92-1.97)
Space group	C 1 2 1
Temperature (K)	100
Rotation range per image (°)	0.5
Total rotation range (°)	360
a, *b*, *c* (Å)	59.03, 47.98, 23.59
α, *β*, *γ* (°)	90.00, 107.13, 90.00

Mosaicity (°)	0.19
Completeness (%)	97.8 (84.5)
CC (1/2)	0.99 (0.97)
R_{merge}	0.029 (0.118)
$\langle I/\sigma(I) \rangle$	25.9 (8.2)
Multiplicity	3.6
No. unique reflections	4744 (275)
R_{work}/R_{free} (%)	14.6/19.3
No. of non-hydrogen atoms	
Protein	558
Ion	1
Water	71
Average B-factors (Å^2)	
Protein	17.5
Ion	10.1
Waters	28.1
R.m.s. deviations	
Bond lengths (Å)	0.004
Bond angles (°)	0.79

Statistics for the highest-resolution shell are shown in parentheses.

$R_{merge} = \sum_{hkl}\sum_j |I_{hkl,j} - < I_{hkl} > |/(\sum_{hkl}\sum_j I_{hkl,j})$

R_{work} / $R_{free} = \sum_{hkl}\left|F_{hkl}^{obs} - F_{hkl}^{calc}\right|/(\sum_{hkl}F_{hkl}^{obs})$; R_{free} was calculated using randomly chosen 10 % fraction of data that was excluded from refinement.

553

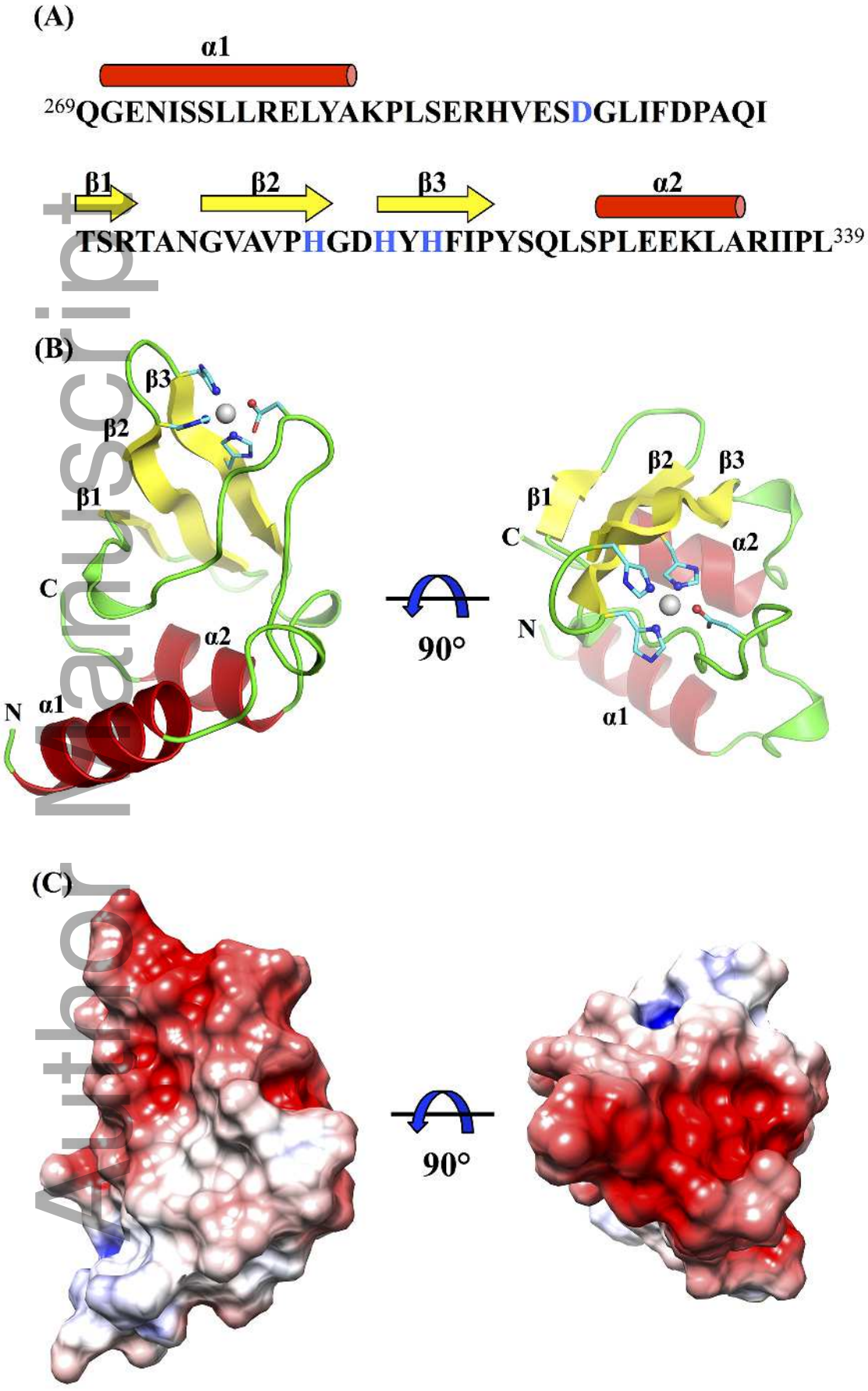

feb2_13122_f1.tif

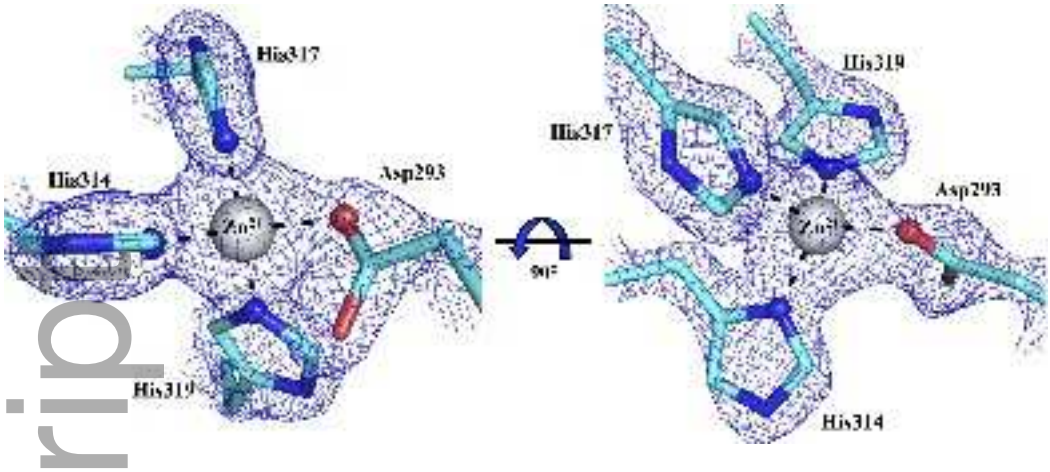

feb2_13122_f2.tif

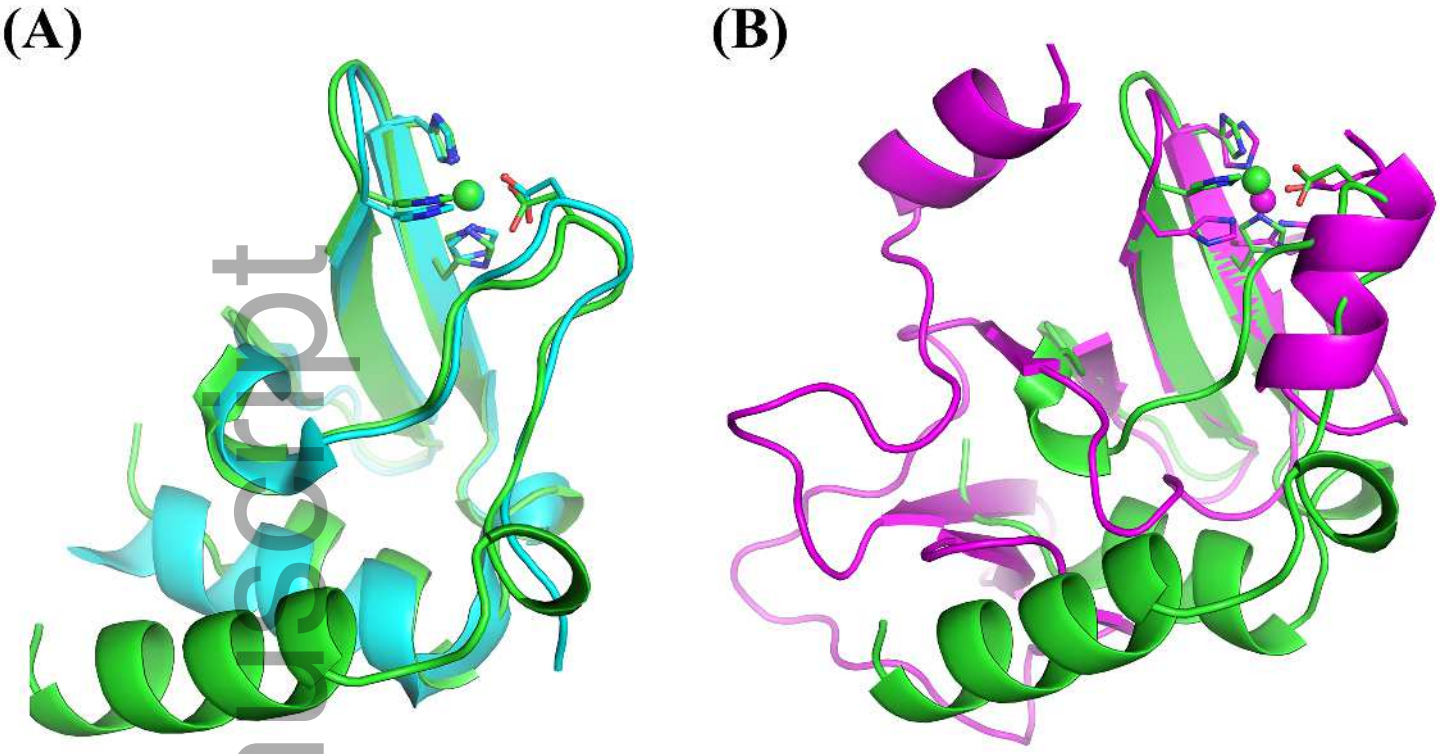

feb2_13122_f3.tif

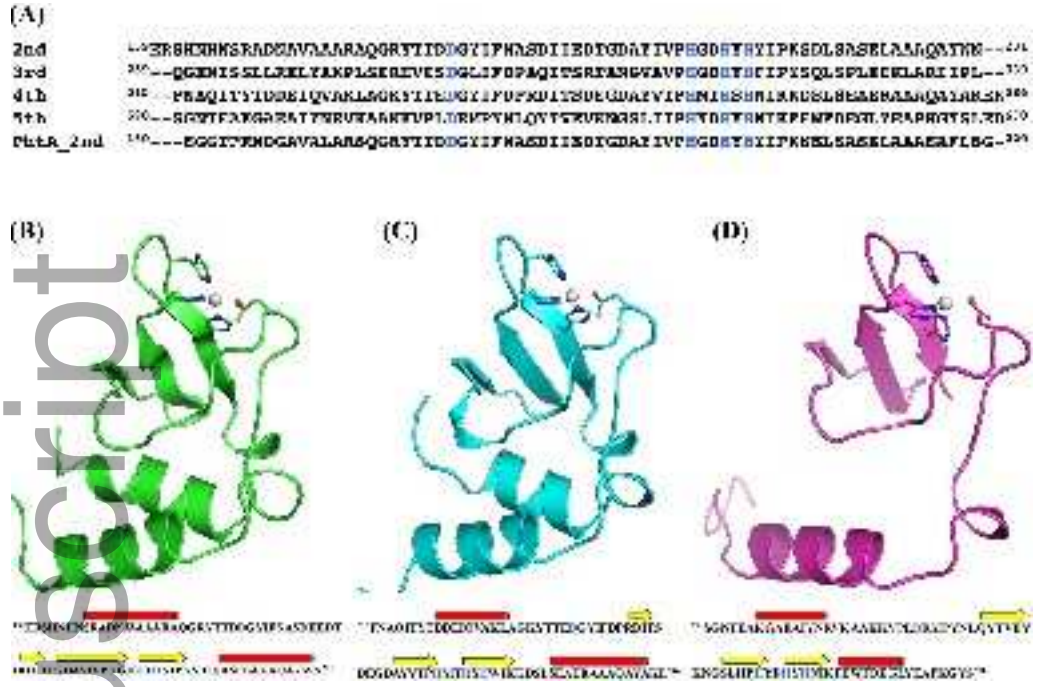

feb2_13122_f4.tif

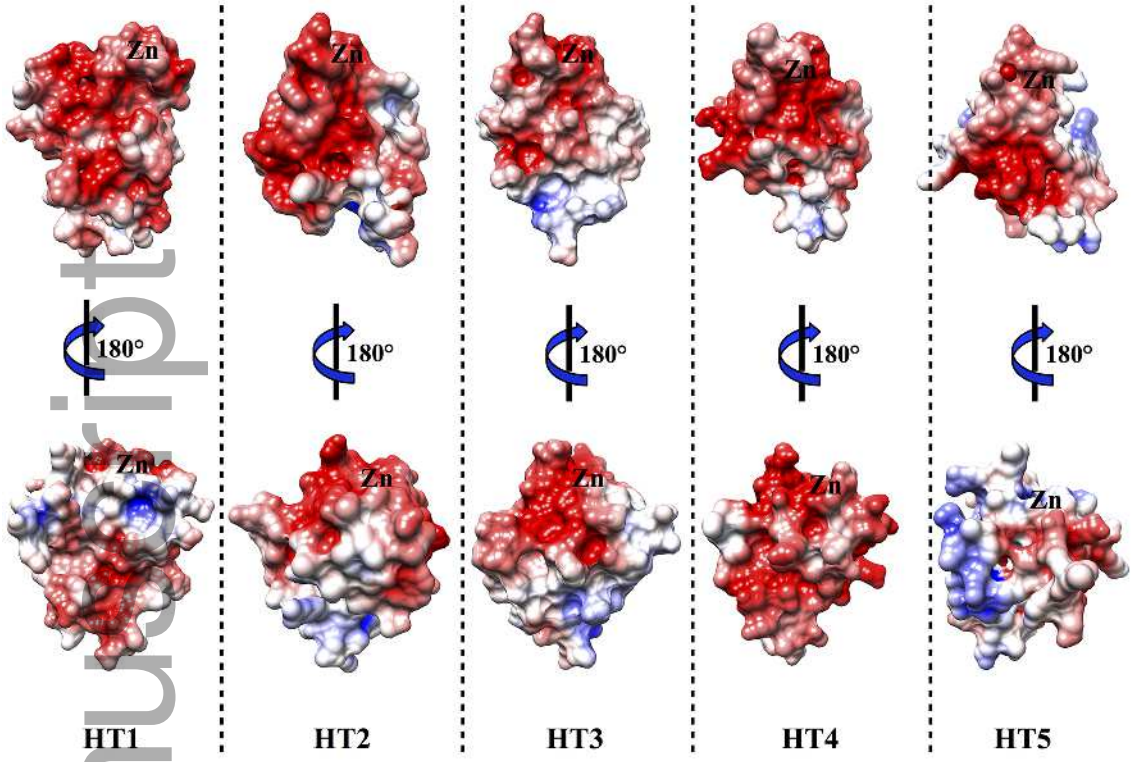

feb2_13122_f5.tif